

gr-qc/9712043
 DAMTP Relativity Group Preprint: DAMTP-R97/56
 Fermilab Preprint: Pub-97/364-A

Persistence Amplitudes from Numerical Quantum Gravity

P. D'Eath,
 DAMTP,
 Cambridge University,
 3 Silver Street,
 Cambridge, CB3 9EW,
 UK

A. Sornborger,
 NASA/Fermilab Astrophysics Group,
 Fermi National Accelerator Laboratory,
 Box 500,
 Batavia, IL 60510-0500
 USA

October 27, 1997

Abstract

The Euclidean quantum amplitude to go between data specified on an initial and a final hypersurface may be approximated by the tree amplitude

$$\exp(-I_{classical}/\hbar), \quad (1)$$

where $I_{classical}$ is the Euclidean action of the classical solution joining the initial and final data. In certain cases the tree amplitude is exact. We study $I_{classical}$, and hence the quantum amplitude, in the case of a spherically symmetric Riemannian gravitational field coupled to a spherically symmetric scalar field. The classical scalar field obeys an elliptic equation, which we solve using relaxation techniques, in conjunction with the field equations giving the gravitational field. An example of the transition from linearity to non-linearity is presented and power law behavior of the action is demonstrated.

PACS numbers 04.20.-q, 04.20.Jb, 04.60.+n

1 Introduction

Much can be learnt in quantum gravity by considering the amplitude to go from an initial to a final configuration of a gravitational and a massless scalar field ϕ . To complete

the specification of the amplitude, one needs to give the time separation between the two spacelike surfaces depicted, together with other data at spatial infinity [1]. If, for example, the time separation is taken to be large, and the bounding data are taken to be weak, then one has a scattering configuration. On the the other hand, the formalism is equally well adapted to studying strong-field amplitudes, as we shall see in this paper, with the help of numerical analysis. One such example concerns the late-time evolution of a radiating black hole. Further examples are provided in quantum cosmology [2-4], where one again needs the strong-field description.

Formally (if the time separation is taken to be Lorentzian) the amplitude is given by a Lorentzian path integral

$$amplitude = \int e^{(iS/\hbar)}. \quad (2)$$

Here the fields $g_{\mu\nu}$ and ϕ in the integration must agree with the boundary data, the intrinsic three-dimensional metric h_{ij} and the scalar field ϕ . Quite apart from convergence questions, there is a more elementary difficulty with the Lorentzian path integral. One might expect the path integral (2) to admit a semi-classical expansion

$$amplitude \sim (A + \hbar A_1 + \dots)exp(iS_c/\hbar). \quad (3)$$

Here S_c denotes the classical action (if such exists) of a classical solution joining the initial to the final data. It is a functional of the boundary data and data at infinity. Similarly the one-loop term A , two-loop term A_1 and so forth depend on the boundary data. Now consider the special case in which the classical geometry is (nearly) flat and one has a massless scalar field between an initial surface $t_1 = 0$ where $\phi = 0$ and a final surface at time t_2 where ϕ is non-zero [4]. The classical solution is

$$\phi(t, \mathbf{x}) = const. \int d^3k \frac{\tilde{\phi}(t_2, \mathbf{k})}{sin(|\mathbf{k}|t_2)} e^{i\mathbf{k}\cdot\mathbf{x}} sin(|\mathbf{k}|t). \quad (4)$$

For general final data, the ‘solution’ is singular because of the poles in the denominator. This is an example of a well-known phenomenon, that the boundary-value problem for a hyperbolic system of equations is not well posed [5]. The expression (4) does, however, make it clear that the boundary-value problem is well-posed if the time-separation is rotated by a small amount $i\epsilon$ into the complex plane[6].

The most natural arena for studying boundary-value problems is within Riemannian geometry, where the Lorentzian time coordinate t is replaced by $t = -i\tau$, with a positive-definite four-metric $g_{\mu\nu}$ and massless scalar field ϕ [7]. One might conjecture that the classical boundary-value problem is well-posed for moderate-sized boundary data; indeed, the numerical methods to be described in Sec. 2 will test this conjecture. The conjecture has been shown analytically to hold for weak (but non-linear) gravitational fields in the absence of a scalar field [8]. The full question of the existence of the coupled nonlinear elliptic Einstein-scalar field equations subject to boundary data is a major unresolved problem in general relativity and partial differential equations. As suggested in the

previous paragraph, one would expect to obtain a Lorentzian amplitude by starting with a Euclidean time interval at infinity, and then rotating the Euclidean time interval towards a Lorentzian time interval. The first treatment of the black-hole evaporation problem by Euclidean methods was by Hartle and Hawking [9]. The original Euclidean approach to quantum cosmology was also due to Hartle and Hawking [3].

For a Riemannian classical geometry, the quantum amplitude will admit the semi-classical expansion

$$\text{amplitude} \sim (A + \hbar A_1 + \dots) \exp(-I_c/\hbar). \quad (5)$$

Here I_c is the classical action for gravity coupled to a massless scalar, and A, A_1, \dots are one-, two-, and higher-loop terms, dependent on the boundary data. Even at the one-loop level, for pure gravity, the Riemannian amplitude is known to be divergent, with divergence linear in the surface invariants [4,10]

$$\begin{aligned} I_1 &= \int d^3x h^{1/2} R_{ij} K^{ij}, \\ I_2 &= \int d^3x h^{1/2} (\text{tr} K)^3, \\ I_3 &= \int d^3x h^{1/2} K_{ij} K^{ij} (\text{tr} K), \\ I_4 &= \int d^3x h^{1/2} K_j^i K_k^j K_i^k. \end{aligned} \quad (6)$$

Here R_{ij} is the Ricci tensor formed from the three-dimensional metric h_{ij} , and K_{ij} is the second fundamental form [11]. (Without boundaries, pure gravity is divergent at two loops and beyond [12].) When a massless scalar field is added, there are again one-loop surface divergences.

All these divergences may be cured by including supersymmetry, providing that one continues to work with surface boundary data given by h_{ij} in the purely gravitational case, and with h_{ij}, ϕ in the gravity-scalar case. From this point of view quantum corrections are ‘soft’ in supersymmetric theories. In fact, provided one sets the appropriate supersymmetric partners to zero on the boundaries, it turns out that the amplitude just has the tree form $\exp(-I_c/\hbar)$, where I_c is the classical action of the original bosonic fields. One may use directly the supergravity calculations of [4]. Note that there was a mistake in the paper [13] which included an earlier discussion of the ideas of [4]. This has been corrected in [4] by the inclusion of the auxiliary fields of supergravity [14], which are of course needed for a complete treatment of supergravity. Another way of motivating this calculation is to understand the action as being derived as an effective action from low-energy superstring theory, in which case we are calculating tree-level amplitudes.

The local boundary conditions used here have been stressed in part because they appear naturally in specifying the path integral. However it is also important to understand that scattering boundary conditions, by contrast, may have very different properties. One obtains scattering boundary conditions by pushing the two spacelike surfaces

off to infinity. Then one takes an infinite product of zero- or one- occupancy harmonic oscillator states. This implies that there is a non-trivial path integral involved in moving between local and scattering boundary conditions, so that it is not surprising that quantum amplitudes with the two types of boundary conditions should be very different. Indeed [15], with scattering boundary conditions the supersymmetric gravity-scalar model is divergent at one loop.

Since the quantum amplitude for the (supersymmetrized) gravity-scalar model is exactly semi-classical, one strategy for computing such amplitudes is clear: set up boundary data and solve the coupled field equations numerically. Include the classical Euclidean action I_c in the numerical calculation, and finally compute the amplitude $exp(-I_c/\hbar)$. The equations for the fields and an expression for the action are presented in Sec. 2. In Sec. 3, we discuss the numerical methods used to find solutions. In Sec. 4, we present the results obtained computationally. And, in Sec. 5, we discuss the results and present our conclusions.

2 Spherical Riemannian Scalar-Gravity Solutions

The Riemannian metric is taken for simplicity in the spherically symmetric form

$$g_{\mu\nu} = diag(e^b, e^a, r^2, r^2 sin^2\theta), \quad (7)$$

in coordinates (t, r, θ, ϕ) , where t is a Riemannian time coordinate and

$$a = a(t, r), \quad b = b(t, r). \quad (8)$$

Notice that for real values of a and b in the metric, the metric is positive definite.

The scalar field is also taken to be spherically symmetric:

$$\phi = \phi(t, r). \quad (9)$$

And the Euclidean action has the form

$$\begin{aligned} I = & -\frac{1}{16\pi} \int d^4x g^{\frac{1}{2}} R \\ & + \frac{1}{2} \int d^4x g^{\frac{1}{2}} (\nabla\phi)^2 \\ & + \text{boundary contributions.} \end{aligned} \quad (10)$$

Here $g = det(g_{\mu\nu})$ and R is the Ricci scalar of $g_{\mu\nu}$. The boundary contributions will later be important and are discussed in Eqs.(2.19-22). The field equations may be written in the form

$$\begin{aligned}
R_{\mu\nu} &= 8\pi\phi_{,\mu}\phi_{,\nu} \\
\partial_\mu(g^{\frac{1}{2}}g^{\mu\nu}\phi_{,\nu}) &= 0
\end{aligned} \tag{11}$$

Here, we have set $G = \hbar = c = 1$.

The Lorentzian version of this problem, with a spherically symmetric scalar field in a Lorentzian spherically symmetric gravitational field, has been studied extensively, leading to many interesting results [16-22].

Explicitly, the Euclidean gravitational field equations are

$$\begin{aligned}
R_{tt} &= \frac{1}{4}e^{-a+b}a'b' - \frac{1}{2}\ddot{a} - \frac{1}{4}\dot{a}^2 \\
&\quad + \frac{1}{4}\dot{a}\dot{b} - \frac{1}{2}e^{-a+b}b'' - \frac{1}{4}e^{-a+b}b'^2 - e^{-a+b}\frac{b'}{r} \\
&= 8\pi\dot{\phi}^2 \\
R_{tr} &= \frac{\dot{a}}{r} \\
&= 8\pi\dot{\phi}\phi' \\
R_{rr} &= \frac{1}{4}a'b' + \frac{a'}{r} - \frac{1}{2}e^{-b+a}\ddot{a} - \frac{1}{4}e^{-b+a}\dot{a}^2 \\
&\quad + \frac{1}{4}e^{-b+a}\dot{a}\dot{b} - \frac{1}{2}b'' - \frac{1}{4}b'^2 \\
&= 8\pi(\phi')^2 \\
R_{\theta\theta} &= \frac{1}{2}e^{-a}a'r - \frac{1}{2}e^{-a}b'r - e^{-a} + 1 \\
&= 0
\end{aligned} \tag{12}$$

The field equations can be simplified, to give (starting with the scalar field equation):

$$\ddot{\phi} + e^{b-a}\phi'' + \frac{1}{2}(\dot{a} - \dot{b})\dot{\phi} + \frac{e^{b-a}}{r}(1 + e^a)\phi' = 0, \tag{13}$$

$$a' = -4\pi r(e^{a-b}\dot{\phi}^2 - \phi'^2) + \frac{(1 - e^a)}{r} \tag{14}$$

$$b' = -4\pi r(e^{a-b}\dot{\phi}^2 - \phi'^2) - \frac{(1 - e^a)}{r} \tag{15}$$

$$\dot{a} = 8\pi r\dot{\phi}\phi' \tag{16}$$

$$\ddot{a} + e^{b-a}b'' + \frac{1}{2}(\dot{a} - \dot{b})\dot{a} - e^{b-a}\frac{(1 - e^a)}{r}(b' + \frac{2}{r}) = 8\pi(\dot{\phi}^2 + e^{b-a}\phi'^2). \tag{17}$$

One can see the general structure of the coupled Riemannian Einstein-scalar equations from this system. The scalar field obeys an elliptic equation (13) which is determined if the gravitational background is known. Conversely, Eqs. (14 - 17) determine a and b if ϕ is known. An effective nonlinearity is present in the elliptic Eq. (13) due to the presence of a and b which involve ϕ . Notice that Eq. (17) is equivalent to Eq. (13) given the constraints, i.e. they are not independent equations.

As the simplest example of a boundary-value problem, one might wish to solve the field equations inside a rectangular boundary, where r runs from the axis $r = 0$ to an outer boundary $r = r_{max}$, and t runs from an initial value t_i to a final value t_f . One normally expects that ϕ and the intrinsic 3-metric h_{ij} would be specified on the boundary [4], in which case one would have $a = a_i$ fixed on the initial surface, a_f on the final surface, and $b = b_f$ on the outer surface. Note also that, for regularity of the initial 3-metric on the initial surface, one should have $a \rightarrow 0$ as $r \rightarrow 0$ on the initial surface. Now consider Eq. (16). By regularity on the axis, $\phi' = 0$ there. Hence $\dot{a} = 0$ along the axis. Hence

$$a(t, r = 0) = 0. \quad (18)$$

This provides another boundary condition.

However, we are unable to solve this version of the boundary-value problem, as the data on the boundaries are overdetermined, we cannot simultaneously fix ϕ and a and b . The correct approach is to fix ϕ on the boundaries, as well as fixing b on the outer boundary (thus fixing the gauge freedom for \dot{b}), then solve Eq. (13) by relaxation [23] and then to compute a and b by integrating the constraint equations (14, 15) iteratively, while checking that the full set (13 - 17) holds after the iteration. There is also one leftover gauge degree of freedom, the value of \dot{b} , which we choose to fix at $r = r_{max}$ by fixing b at r_{max} .

The classical action for our system of equations resides on the boundary. It is

$$I_c = -\frac{1}{8\pi} \int d^3x h^{\frac{1}{2}} tr K + \frac{1}{2} \int d^3x h^{\frac{1}{2}} \phi \frac{\partial \phi}{\partial n}. \quad (19)$$

The integral is taken over all bounding surfaces, with intrinsic metric h_{ij} and $h = \det(h_{ij})$. Here K_{ij} is the Euclidean second fundamental form [4], taken with respect to the outward normal, and $tr K = h^{ij} K_{ij}$. For the upper surface $t = t_f$ (say), one finds

$$I_f = -\frac{1}{4} \int dr r^2 e^{(a-b)/2} \dot{a} + 2\pi \int dr r^2 e^{(a-b)/2} \phi \dot{\phi}, \quad (20)$$

with a corresponding expression for I_i in which the minus and plus signs are reversed. There is also a contribution from the outer boundary at $r = r_f$, which is near $r = \infty$ in our case. It is [4]

$$I_\infty = MT, \quad (21)$$

where M is the mass of the space-time and T is the proper Euclidean time-interval between the initial and final surfaces. Hence the total classical Euclidean action is

$$\begin{aligned}
I_{total} = & -\frac{1}{4} \int_{top} dr r^2 e^{(a-b)/2} \dot{a} + 2\pi \int dr r^2 e^{(a-b)/2} \phi \dot{\phi} \\
& + \frac{1}{4} \int_{bottom} dr r^2 e^{(a-b)/2} \dot{a} - 2\pi \int dr r^2 e^{(a-b)/2} \phi \dot{\phi} \\
& + MT.
\end{aligned} \tag{22}$$

3 Numerical Methods

We use the standard artificial time method for relaxing the elliptic equation. This relaxation method uses the artifice of introducing a diffusive term to the elliptic equation. The diffusive term gradually relaxes to zero and one is left with a solution to the elliptic operator of interest.

With this relaxation method, we solve the equation

$$\partial_\tau \phi + L(\phi, a, b, \dot{a}, \dot{b}) = 0 \tag{23}$$

where τ is an artificial time coordinate, and L is the nonlinear elliptic operator for which we desire a solution. We solve the equation by discretising in the artificial time and also imaginary time and space, then integrating the equation in time. For a linear elliptic operator discretised in this manner, there is a constraint on the allowed size of the integration timestep. For instance, for solving the heat equation, the constraint is $\Delta t \leq (\Delta x)^2/2$. For a nonlinear elliptic operator, the timestep must typically be kept substantially smaller, such that the integration is effectively linear. In our integrations, for a simulation volume of 0.8, we took $\Delta t = 0.00005$, typically. The small value of timestep needed in our case is a measure of the non-linearity of our problem.

After one integration of Eq. (23) where L is given by (13), we use Eq. (14) to integrate a radially outwards from the axis where $a = 0$. For a radius of one gridpoint out from the axis we are forced to approximate Eq. (14) in order to avoid problems from divergences due to small values of r . At large r , the solution for a will be dominated by the non- ϕ part of Eq. (14). The solution to this will be a Schwarzschild solution, so that one will have $a \sim 2M/r$ as $r \sim \infty$, where M is the mass of the space-time. One also integrates Eq. (15) to derive values for b inwards from the outer boundary to the axis. Then one iterates this procedure until ϕ, a, b converge (if this occurs), checks that the remaining equations (16, 17) hold, and evaluates the action.

4 Results

We have run a number of integrations with simulation volume sides of 0.8 in units where $G = \hbar = c = 1$. $\phi(r)$ was set to

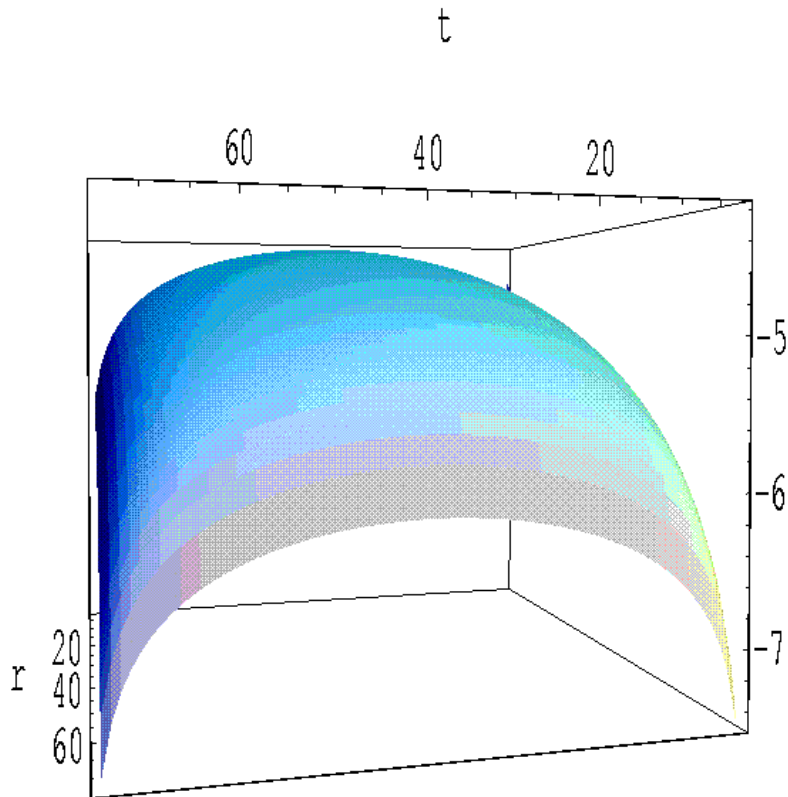


Figure 1: A plot of the \log_{10} of the error in calculation of the elliptic scalar field equation for ϕ on a 75^2 grid for $d = 1.0$.

$$\phi = \frac{d}{8\pi} \exp(-100r^2), \quad (24)$$

(where d is a parameter) on the initial and final time surfaces. Thus, we have identical values of ϕ at opposite points on the initial and final surfaces. Note here that the outer boundary at $r = r_{max} = 0.8$ is fairly close to $r = \infty$ in terms of the asymptotic fields. This means that the action is simple to calculate at the r_{max} boundary.

We performed integrations on grids with 25^2 , 35^2 , 50^2 , 75^2 and 100^2 gridpoints. We also performed a few integrations on a 200^2 grid, however, these calculations were very time consuming.

To claim a solution, we required that the elliptical scalar field equation be zero to one part in one hundred thousand. We also checked that the constraint equations were satisfied. In general, the elliptical equation converged to 10^{-5} up to some value of the

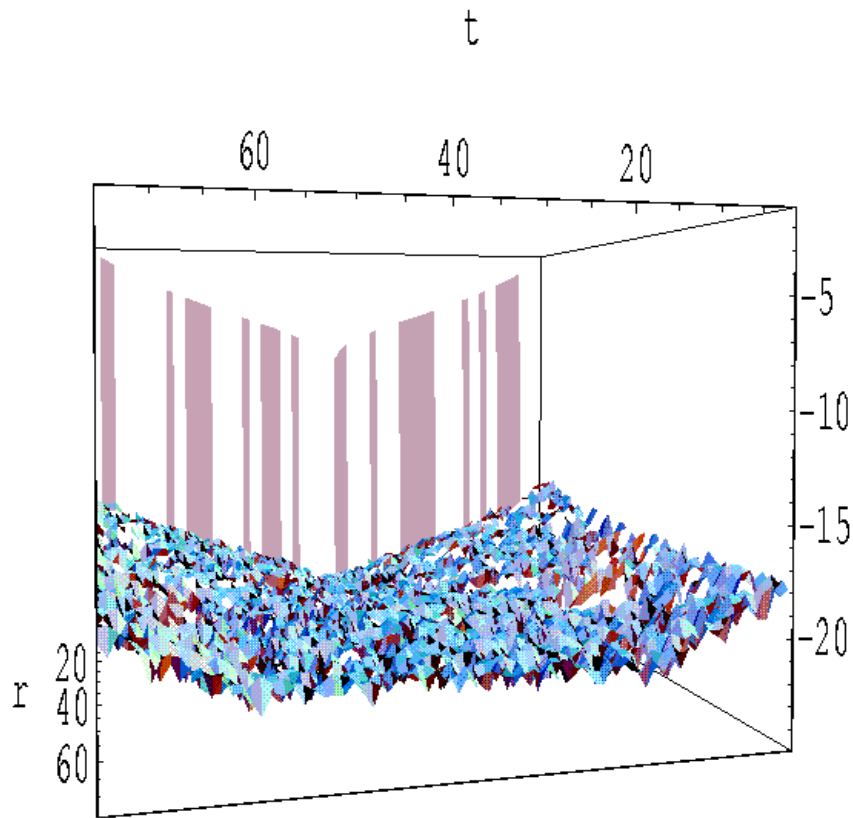


Figure 2: A plot of the \log_{10} of the error in calculation of the constraint equation for a' on a 75^2 grid for $d = 1.0$.

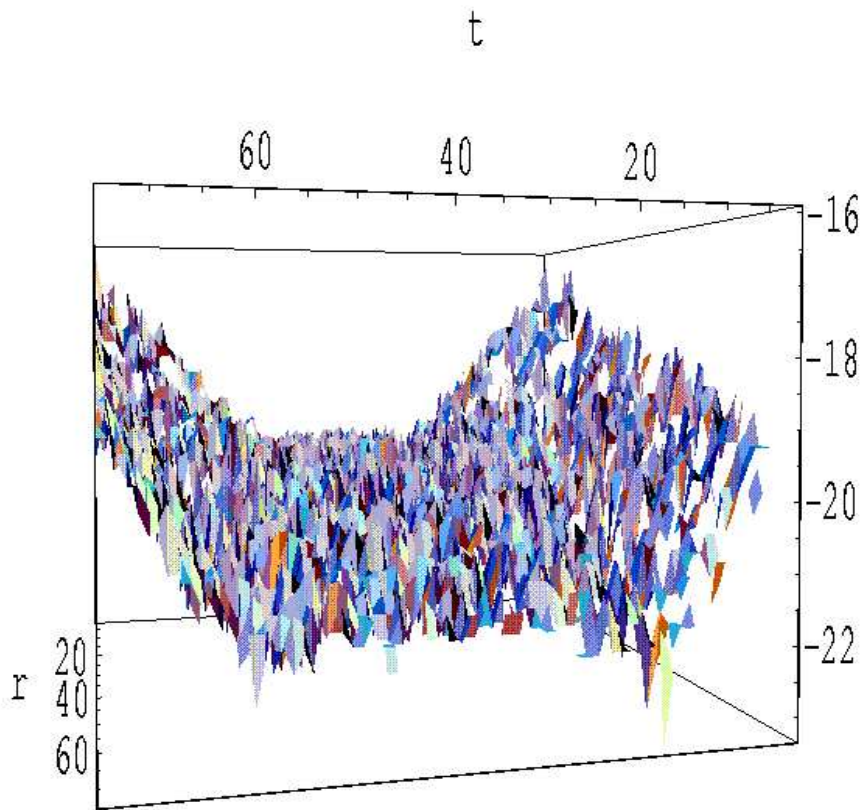


Figure 3: A plot of the \log_{10} of the error in calculation of the constraint equation for b' on a 75^2 grid for $d = 1.0$.

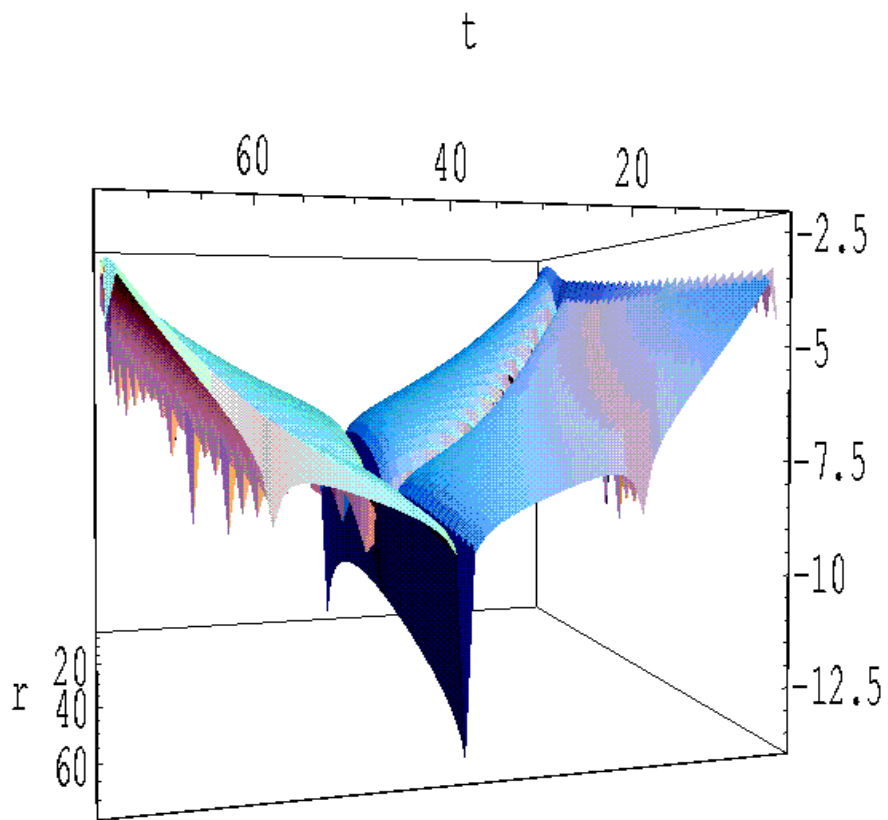


Figure 4: A plot of the \log_{10} of the error in calculation of the constraint equation for \dot{a} on a 75^2 grid for $d = 1.0$.

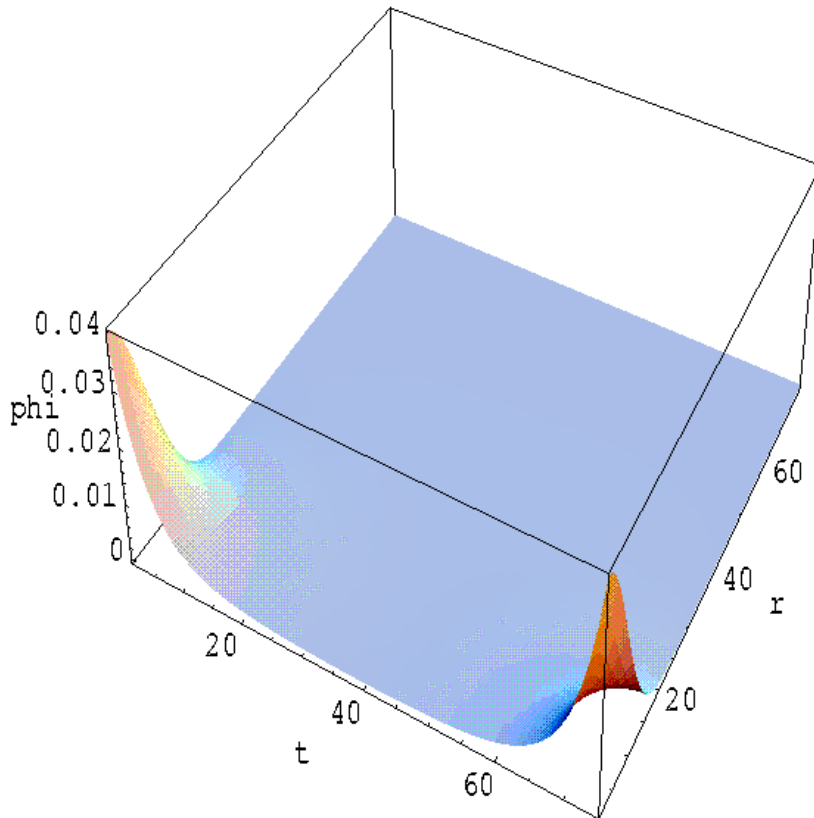


Figure 5: The solution for field ϕ on a 75^2 grid. Notice the time symmetry of the solutions here and in figures (6) and (7), this indicates that our numerical methods are obeying the symmetry of the equations.

parameter d . Smaller grids tended not to converge for smaller values of d than larger grids. Because the constraint equations are just ordinary differential equations integrated forwards or backwards in the r direction on the grid, they had roughly constant errors. In figures (1), (2), (3) and (4), we plot the \log_{10} of the errors for the solutions of equations (13), (14), (15) and (16) for a solution on a 75^2 mesh with $d = 1.0$. Note that the error for ϕ is everywhere less than 10^{-5} . The errors for the constraints on a' and b' are negligible (parts of the plotted surface that are missing correspond to errors of 0 to within machine accuracy). And the error for the constraint on \dot{a} is less than $10^{-2.5}$. Significantly, the error for the constraint equation for \dot{a} is largest where spurious oscillations occur in the solution (see below).

In figures (5), (6) and (7) the solution for $d = 1.0$ is shown on a 75^2 grid. Notice the time symmetry in ϕ as well as e^a and e^b . This is evidence that our relaxation method

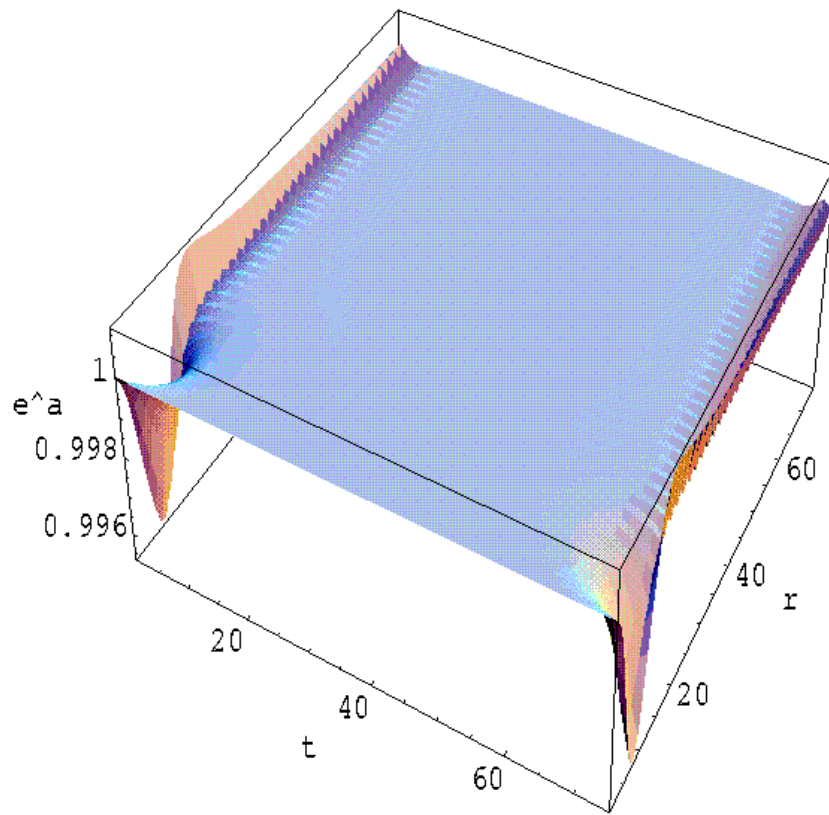


Figure 6: The solution for metric field e^a on a 75^2 grid

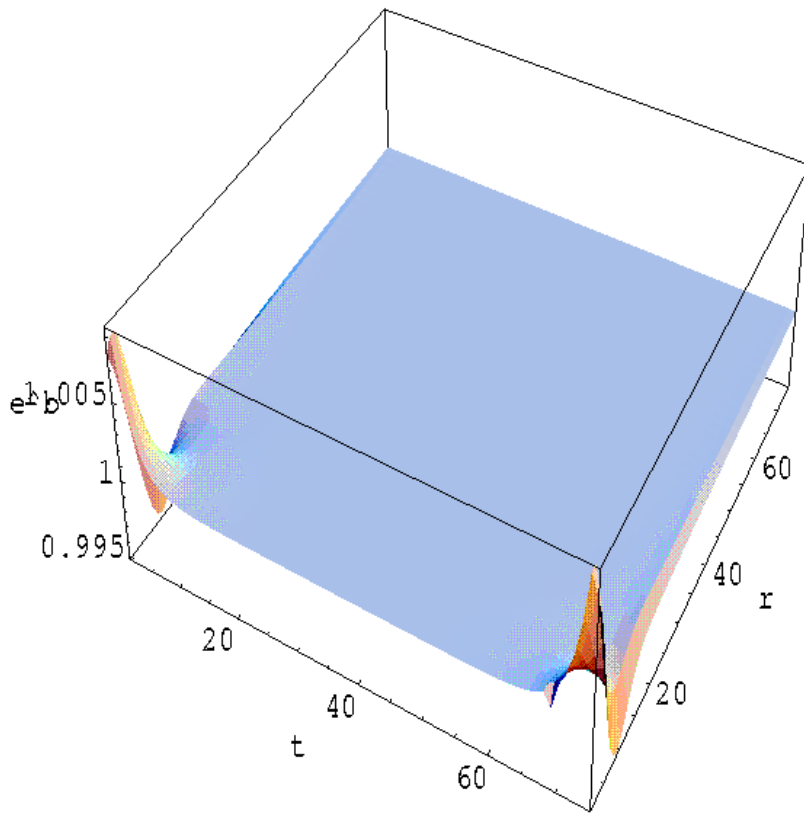


Figure 7: The solution for metric field e^b on a 75^2 grid

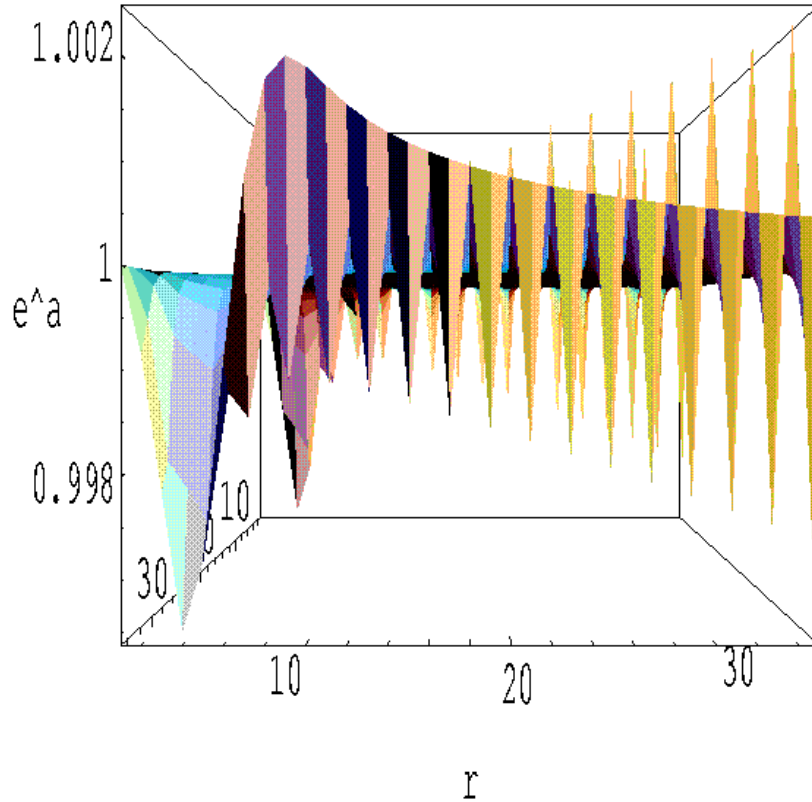


Figure 8: The solution for metric field e^a on a 35^2 grid. This is a side view. The amplitude of the spurious oscillations on this coarse grid decrease as the grid resolution increases in figures (9) and (10)

preserves the time symmetry of the equations.

In all numerical solutions, we find spurious oscillations near, but not at the boundary, as presented in figures (8), (9) and (10). The oscillations occur only in the a metric component. Notice from the figures that the amplitude of the oscillations decreases with finer meshes, with oscillations on the 200^2 grid substantially reduced with respect to the coarser grids. Interestingly, the spurious oscillations do not appreciably affect the value of the action. This is because the oscillations are integrated over in calculating the action. A feature that does affect the action calculation can be seen in the depth of the dip near $r = 0$. This feature ranges in value from 0.9965 for the 35^2 solution, to 0.9947 for the 200^2 solution. In figure (11), we see how this influences the value of the action.

In figure (12), we plot \log_{10} of the action as a function of \log_{10} of the parameter d . The resulting power law with slope 2 is quite striking. In this figure, we have actually plotted

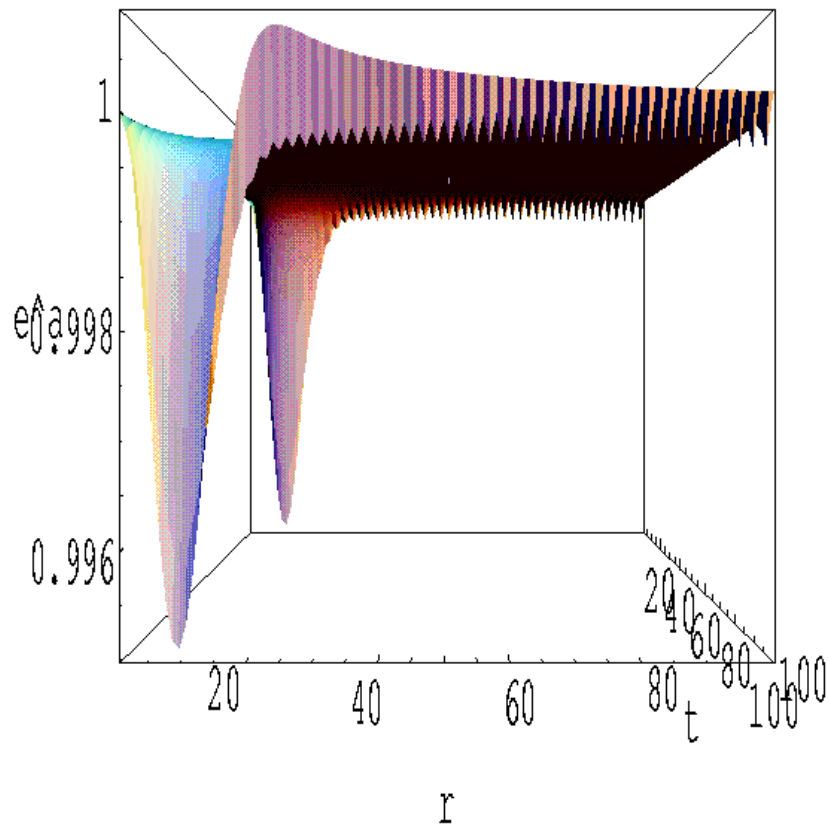


Figure 9: The solution for metric field e^a on a 100^2 grid.

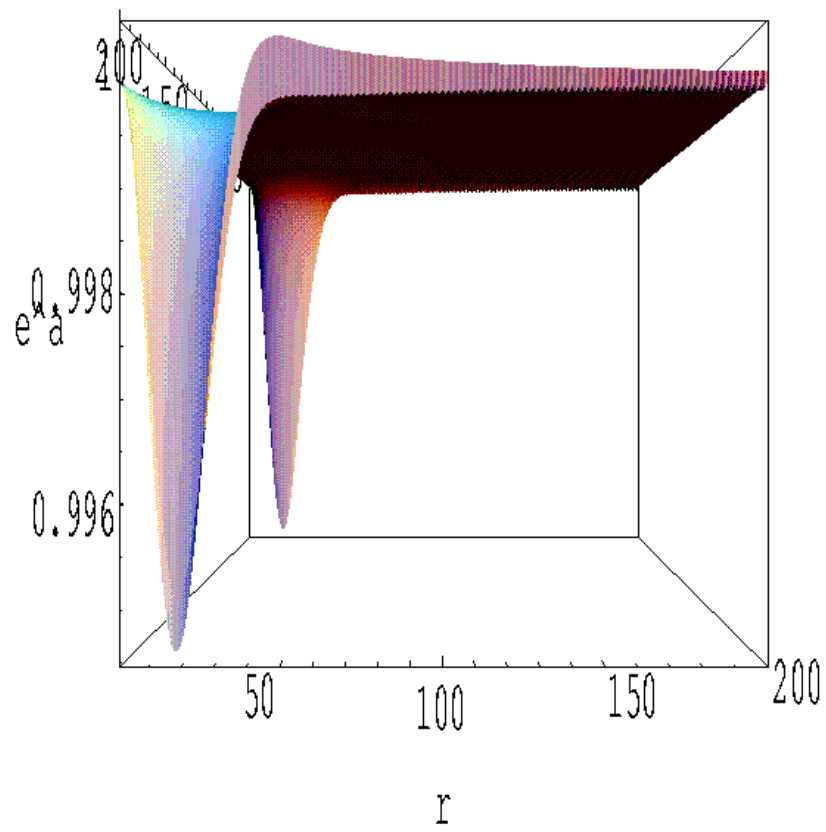


Figure 10: The solution for metric field e^a on a 200^2 grid.

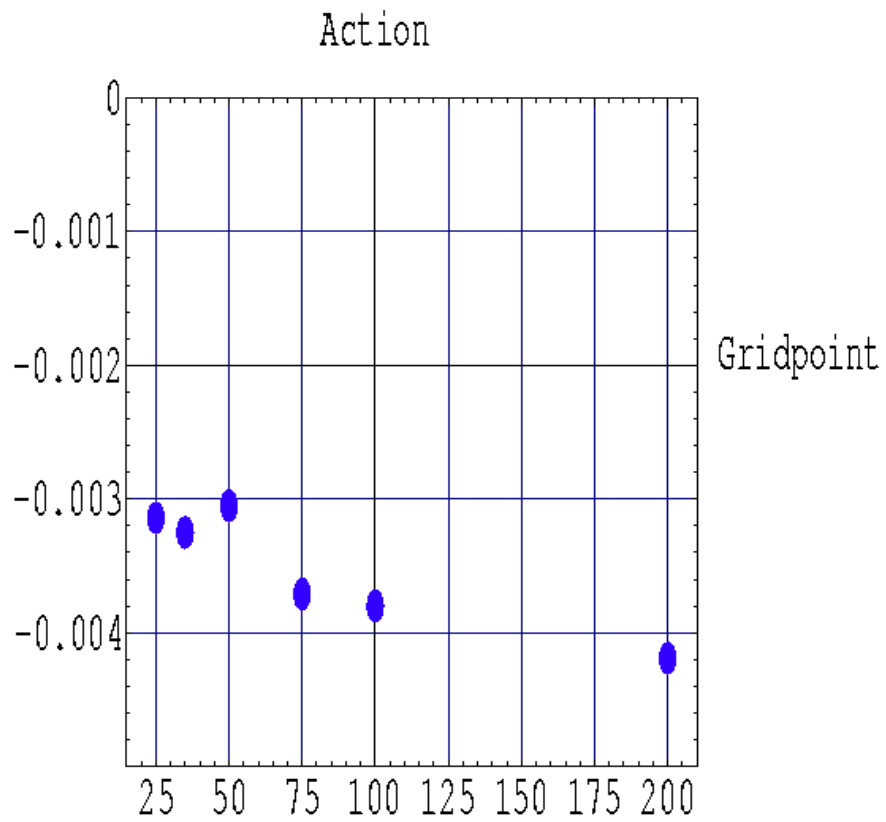


Figure 11: In this plot, we show the dependence of the value of the action on the resolution of the numerical integration.

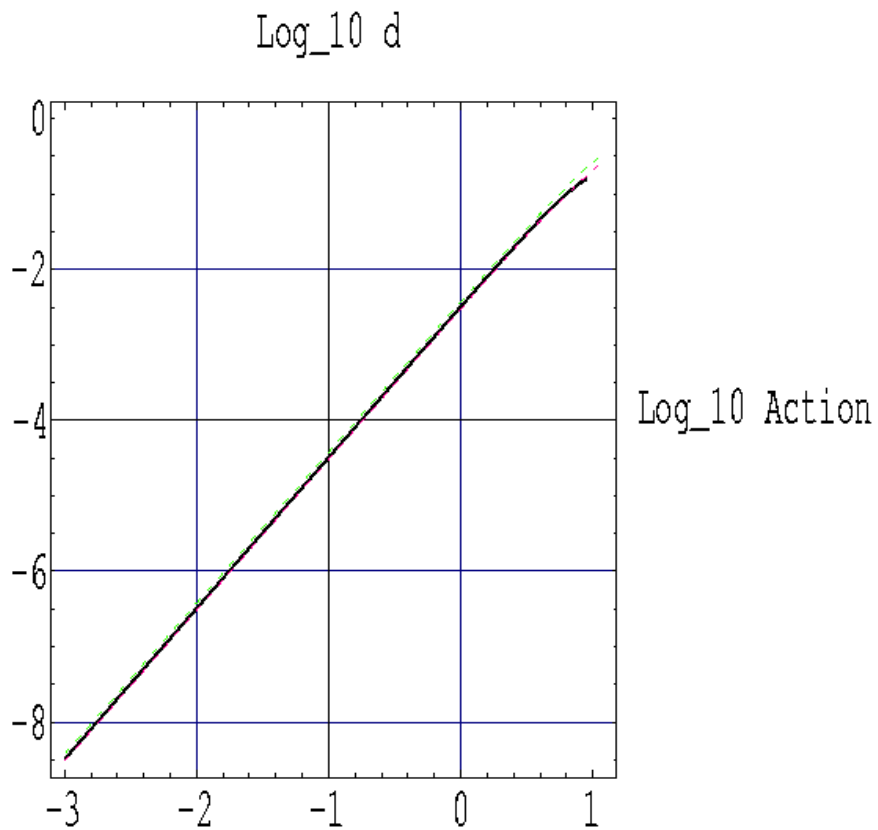


Figure 12: Here, we plot \log_{10} of the absolute value of the action as a function of \log_{10} of parameter d for gridsizes 35^2 , 50^2 and 100^2 . Thus, $I \sim -d^2$. This behavior shows the expected increase of persistence amplitude with binding energy of the system.

the absolute value of the action, which means that the action $I \sim -d^2$. The decrease of the action with increasing d is a natural result of the increased binding energy of the system. As we enter the nonlinear regime, we would expect that the power might change, and, indeed, we do begin to see a bend for larger values of d in the plot. However, the bend decreases with increasing grid resolution. For various grid sizes L , we find the slope n to be:

L^2	n	
35^2	1.956	(25)
50^2	1.968	
100^2	1.971	

The straightening of the bend in the action is due to the better resolution of the dip in the metric functions on higher resolution meshes. The tendency for the slope to approach 2 for high resolution meshes, may indicate that the actual solution has a slope of 2 exactly, even well into the nonlinear regime. However, we have only shown the tendency, and cannot prove this assertion.

5 Discussion and Conclusions

In this paper, we have studied amplitudes for the spherically symmetric system of a scalar field coupled to gravity. We have looked at amplitudes for the field to persist in its current state. We have taken the field to have support primarily near the symmetry axis, with amplitude parametrised by the parameter d .

What we can say from our study, is that the Euclidean action is well-behaved, negative and obeys obvious power law behaviour, with the action $I \sim -d^2$. There are indications that the power behavior remains the same into the nonlinear regime. The decrease of the action with increasing d is a result of the increasing binding energy of the system as the scalar field gets large. This result is also familiar from the understanding of black hole evaporation: massive black holes radiate more than less massive black holes. The persistence amplitudes that we calculate show the opposite side of the coin: a massive scalar field is more likely to retain its integrity than a less massive scalar field.

The solutions that we obtain are all time symmetric and largely slowly varying (for values of d which we have been able to probe) outside of regions near the initial and final times, where they vary rapidly.

From the numerical solutions that we have obtained, it is clear that more work needs to be done exploring the strong-field Euclidean gravity equations. The obvious direction to go numerically is to develop a mesh-refinement code. A mesh-refinement code would increase the efficiency of the calculation by focusing on regions of the solution that are varying quickly, thus decreasing the computational time needed for a given resolution, and increasing the resolution of the solution.

This conclusion from our work on fixed meshes is in accord with what we know of

critical behavior from work on the Choptuik problem. Adaptive meshes with an effective resolution of billions of gridpoints were necessary to see the full nonlinear critical behavior in the Lorentzian case.

As well as refining the numerical approach to this problem, we plan to investigate more different kinds of solution. In particular, solutions which are not time symmetric, in order to investigate amplitudes for evaporative and condensive processes.

6 Acknowledgements

The generous help of Neil Cornish, Gary Gibbons, Rufus Hamade, Stephen Hawking, Christopher Hunter, Stuart Rankin and John Stewart is gratefully acknowledged. A.S. acknowledges the receipt of PPARC grant number GR/L21488 and support from the DOE and NASA grant NAG 5-2788 at Fermilab.

7 References

- [1] Teitelboim, C., (1977) Phys.Lett.B69, 240
- [2] DeWitt, B.S., (1967) Phys.Rev.160, 1113
- [3] Hartle, J.B., and Hawking, S.W., (1983) Phys.Rev.D28, 2960
- [4] D'Eath, P.D., (1996) Supersymmetric Quantum Cosmology (Cambridge: Cambridge University Press)
- [5] Garabedian, P.R., (1964) Partial Differential Equations (New York: Wiley)
- [6] Feynman, R.P., and Hibbs, A.R., (1965) Quantum Mechanics and Path Integrals (New York: McGraw-Hill)
- [7] Hawking, S.W., (1979) in General Relativity. An Einstein Centenary Survey, ed. Hawking, S.W. and Israel, W. (Cambridge: Cambridge University Press)
- [8] Reula, O., (1987) Max-Planck-Institut fur Astrophysik preprint MPA 275
- [9] Hartle, J.B., and Hawking, S.W. (1976) Phys.Rev.D13, 2188
- [10] Moss, I.G. and Poletti, S.J., (1994) Phys.Lett.B333, 326
- [11] Misner, C.W., Thorne, K.S. and Wheeler, J.A., (1973) Gravitation San Francisco: Freeman)
- [12] Goroff, M.H. and Sagnotti, A., (1985) Phys.Lett.B160, 81
- [13] D'Eath, P.D. (1994) Phys.Lett.B321, 368
- [14] Wess, J. and Bagger, J. (1992) Supersymmetry and Supergravity (Princeton: Princeton University Press)
- [15] van Nieuwenhuizen, P. (1981) Phys.Rep.68, 189
- [16] Choptuik, M.W. (1993) Phys.Rev.Lett.70, 9
- [17] Choptuik, M.W. (1994) in Deterministic Chaos in General Relativity ed. Hobill, D. et. al. (New York: Plenum)
- [18] Christodoulou, D. (1991) Commun. Pure Appl. Math. 44, 339
- [19] Christodoulou, D. (1993) Commun. Pure Appl. Math. 46, 1131

- [20] Garfinkle, D. (1994) Phys. Rev.D51, 5558
- [21] Gundlach, C., Price, R. and Pullin, J. (1994) Phys. Rev.D49, 890
- [22] Hamade, R.S. and Stewart, J.M. (1996) Class. Quantum Grav.13, 497
- [23] Press, W.H. et. al. (1994) Numerical Recipes (Cambridge: Cambridge University Press)
- [24] Iserles, A. (1996) A First Course in the Numerical Analysis of Differential Equations (Cambridge: Cambridge University Press)